ACS APPLIED MATERIALS & INTERFACES

Research Article

www.acsami.org

Protective Ligand Shells for Luminescent SiO_2-Coated Alloyed Semiconductor Nanocrystals

María Acebrón,[†] Juan F. Galisteo-López,[‡,§] Daniel Granados,[†] Javier López-Ogalla,[†] José M. Gallego,[†,‡] Roberto Otero,[†,∥] Cefe López,[‡] and Beatriz H. Juárez*[,†,⊥]

[†]Instituto Madrileño de Estudios Avanzados en Nanociencia (IMDEA-Nanoscience), Cantoblanco 28049, Madrid, Spain

[‡]Instituto de Ciencias de Materiales de Madrid (ICMM), Consejo Superior de Investigaciones Científicas (CSIC), Calle Sor Juana Inés de la Cruz 3, 28049 Cantoblanco, Madrid, Spain

[∥]Departamento de Física de la Materia Condensada and Instituto Nicolás Cabrera, Universidad Autónoma de Madrid, 28049 Cantoblanco, Madrid, Spain

[⊥]Departamento de Química-Física Aplicada, Universidad Autónoma de Madrid, 28049 Cantoblanco, Madrid, Spain

Supporting Information

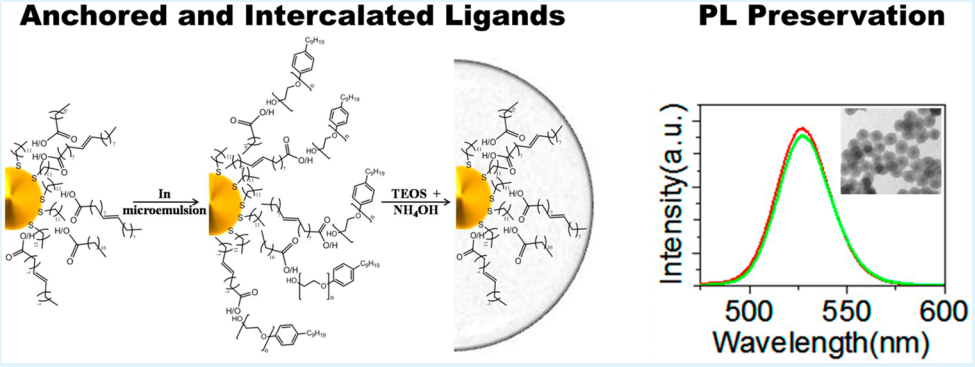

ABSTRACT: SiO_2 encapsulation of alloyed CdSeZnS nanocrystals (NCs) shows differences in terms of optical properties and luminescence quantum yield, depending on the surface composition, size, and ligand content. In this work, emphasis has been placed on the fine control required to obtain luminescent SiO_2 encapsulated NCs by studying the role of oleic acid (OA), stearic acid (SA), and dodecanethiol (DDT) ligands on the alloyed NCs. While the use of anchored DDT molecules is essential to preserve the optical properties, intercalated OA and SA play a critical role for SiO_2 nucleation, as stated by ^{1}H NMR (including DOSY and NOESY) spectroscopy. These results emphasize the importance of surface chemistry in NCs; it is crucial to control their reactivity, and therefore their impact, in different applications, from optics to biomedicine.

KEYWORDS: *microemulsion, silica encapsulation, alloyed semiconductor nanocrystals, colloidal quantum dots, luminescence quantum yield, surface chemistry*

INTRODUCTION

Semiconductor nanocrystals (NCs), also called colloidal quantum dots, have attracted much attention, especially for their tunable optical properties and optical stability.[1] Their production has benefited from relatively straightforward wet chemical methods that allow them to be produced on the milligram to gram scales, mainly in organic media. The interest of NCs encapsulation in SiO_2 includes their conversion in water-soluble NCs, the addition of functionalities for further applications (e.g., biological) and the decrease of their toxicity (as SiO_2 may block the release of toxic heavy metal ions).[2−4] One of the most popular methodologies to cover NCs with SiO_2 is to place them in a reversed microemulsion, where small droplets of water play the role of nanoreactors. The controlled synthesis in different microemulsion media can be used to obtain SiO_2-covered NCs, either individually[5−7] or in bunches.[8,9] Koole et al.[10] studied the influence of different ligands and the order of addition of the reactants in the SiO_2 encapsulation reaction. This order is important because each reactant has a different effect on the NC surface chemistry. In fact, the majority of the reported work indicates that SiO_2 encapsulation proceeds with a concomitant reduction of the initial photoluminesce (PL) quantum yield (QY) due to generation of nonradiative paths. Thus, a major challenge is the encapsulation in SiO_2 without lessening their optical properties.

In this work, we report the effect of SiO_2 encapsulation on the optical properties of alloyed CdSeZnS NCs. While the SiO_2 encapsulation of NCs composed of a simple core or core−shell

Received: January 27, 2015
Accepted: March 10, 2015
Published: March 10, 2015

DOI: 10.1021/acsami.5b00820
ACS Appl. Mater. Interfaces 2015, 7, 6935−6945

structure has been previously studied,[5−16] SiO_2 encapsulation of alloyed semiconductor NCs remains largely unexplored. Alloyed NCs have been proven to be robust and efficient systems as a result of a graded combination of the elements comprising the NCs from the inner core to the outer shell, thus reducing lattice mismatches in an otherwise well-defined core−shell structure.[17] The main disadvantage of alloyed NCs is in connection with the relatively poor control over the gradient and surface composition, which may differ from NC batches produced under slightly different precursor concentrations. Thus, understanding the factors affecting the SiO_2 encapsulation mechanism in alloyed systems turns out to be essential to preserve the optical properties and to avoid PL quenching. To exemplify this statement, we study the SiO_2 encapsulation of different alloyed NCs in a microemulsion medium. As a result, we introduce a methodology that allows covering NCs with SiO_2 while preserving or even increasing the initial QY.

The reversed microemulsion includes hexane as the oil component, a surfactant (poly(5)oxyethylene-4-nonylphenylether, Igepal CO-520) and water. In general, it is accepted that covering NCs in microemulsions involves ligand exchange of the initial NCs ligands with the surfactant, the SiO_2 precursor (usually tetraethyl orthosilicate, TEOS), or both.[6,11,16] In this scenario, a displacement of the original ligands could be the reason for the PL decrease. To understand the hydrolysis of TEOS, other authors rather claim interactions between the alkyl chains of the microemulsion surfactant and the ligands capping the NC surface.[3] It has also been proposed that the high affinity of TEOS for the aqueous microemulsion droplets is responsible for the coverage reaction, regardless of the microemulsion surfactant affinity for the NCs surface.[18] In this work we derive some suggestions to help understand the mechanism of this coverage reaction from ^1H NMR spectroscopy including diffusion ordered (DOSY) and nuclear overhauser effect (NOESY) spectroscopy. The results allow us to conclude that, in our system, nonanchored oleic acid (OA) and/or stearic acid (SA) ligands get interlinked within tightly anchored 1-dodecanothiol (DDT) molecules and also interact with the surfactant molecules (Igepal). Thus, the hydrolysis reaction takes place on the ligand shell and does not involve displacement of the DDT ligands. The effect of OA/SA and DDT on the coverage depends on the size and surface composition of the alloyed CdSeZnS NCs, which underlines the complexity of factors influencing the coating reaction. We introduce a methodology in which previous incubation of NCs in DDT and then in OA/SA preserves or even increases the initial photoluminesce QY after SiO_2 encapsulation.

EXPERIMENTAL SECTION

Chemicals. Cadmium oxide Puratronic (CdO, 99.998%), zinc stearate (Zn 12.5−14% powder), selenium (99.999%, powder), and sulfur (99.9%, powder) were purchased from Alfa Aesar. Trioctylphosphine (TOP, 90%), oleic acid (OA, 90%), stearic acid (SA, 98.5%), 1-octadecene (ODE, 90%), and 1-dodecanthiol (DDT >98%), hexane (≥99%), Igepal CO-520 (poly(5)oxyethylene-4-nonylphenylether), ammonia (NH_4OH 28 wt %), and deuterated chloroform (99.96%) were purchased from Sigma-Aldrich. Acetone (99.5%), absolute ethanol (99.8%), and hydrochloric acid (37%) were purchased from Panreac. Tetraethyl orthosilicate (TEOS 98%) was purchased from ACROS Organics, and zinc stearate dihydrate was purchased from Scharlau. Nitric acid (65%) was purchased from AnalaR NORMAPUR. All chemicals were used directly without further purification.

General Procedure for the Synthesis of Graded NCs. The synthetic procedure is based on a method previously reported by Bae et al.[19] with some modifications. For the reaction, 0.05 mmol of CdO and 2 mmol of zinc stearate were placed in a 50 mL three-necked round flask, with 2.5 mL of OA. The mixture was heated to 150 °C and degassed for 30 min. Then, 7.5 mL of ODE were added, and the solution was further heated to 300 °C under N_2 atmosphere. At this temperature, a clear solution was observed containing $Cd(OA)_2$ and $Zn(OA)_2$ complexes. When the temperature stabilized, 1 mL of a solution prepared from 0.8 mmol of Se and 5.5 mmol of S in 4 mL of TOP was quickly injected. Immediately after the injection, the temperature went down 10 degrees. The NCs were grown for 2−10 min. After this time, the flask was cooled, and 1.5 mL (6 mmol) or 0.25 mL (1 mmol) of DDT was added to the solution. For the purification, redispersion in hexane and subsequent centrifugation cycles with acetone were carried out (four times).

General Procedure for Silica Encapsulation. To encapsulate the NCs, we carried out a microemulsion method described in previous works[5,10−16] with slight modifications. 0.5 mL of a NCs solution (optical density, OD = 0.036) was mixed with a microemulsion composed by 0.61 g of Igepal-CO 520, 62 μL of ultrapure water, and 11 mL of hexane. This emulsion was sonicated for 15 min to produce good dispersions of the NCs without aggregation. After that, 100 μL of TEOS were added under vigorous stirring (750 rpm). After 30 min the hydrolysis and condensation of TEOS was triggered upon injection of 30 μL of NH_4OH. The mixture was stirred for 24 h. Afterward, the samples were washed 10 times in cycles of centrifugation and ultrasonication (the first one in acetone and the subsequent ones in absolute ethanol).

Incubation Prior to Silica Encapsulation. Incubation involves the addition of certain amounts of DDT, OA, or SA (between 5 and 50 μL) to the NCs dispersions in hexane (0.5 mL of a NCs solution; OD = 0.036) prior to the mixing with the microemulsion. All incubations are performed for 24 h while stirring. After this time, Igepal, water, TEOS, and NH_4OH were added following the same procedure described above.

CHARACTERIZATION

Optical absorption measurements were carried out using a Varian Spectrophotometer Cary 50. Photoluminescence (PL) spectra were recorded in a spectrofluorometer Horiba Jobin Yvon Fluoromax-4 and QY values were measured in a spectrofluorometer Fluorolog TCSPC Horiba Jobin Yvon using an integrating sphere Quanta φ Horiba Scientific. This equipment assures a good comparison between samples composed of NCs exhibiting different sizes and possible light scattering from the SiO_2 shell (although not significant for the SiO_2 shells reported here).

High-resolution transmission electron microscopy (HRTEM) images were obtained in a JEOL 2100F operating at 200 kV. Size distribution data were obtained by measuring the NC sizes from TEM images. At least 100 NCs were measured in each sample.

X-ray photoelectron spectroscopy (XPS) measurements have been performed using a Synchrotron source ($h\nu$ = 920 and 720 eV) at BESSY II, Berlin. Spectra for Cd 3d, Se 3d, Zn 3d, and S 2p were recorded using pass energies of 20 and 50 eV. The binding energies were referenced to the Cd $3d_{5/2}$ core level at 405.2 eV.

Lifetime measurements were performed with a Time Correlated Single Photon Counting card (Becker & Hickl SPC-300). The NCs or SiO_2 covered NCs were placed in a quartz cuvette and pumped with a tunable laser (OPerA-Solo from Coherent) delivering 150 fs long pulses with λ = 355 nm and a repetition rate of 1 kHz. Emission was collected with an

DOI: 10.1021/acsami.5b00820
ACS Appl. Mater. Interfaces 2015, 7, 6935−6945

optical fiber and passed through a monochromator prior to detecting it with an avalanche photodiode.

NMR samples were dried with a N_2 flux and prepared in deuterated chloroform. ^{1}H NMR experiments of Figures 5 and 8 and Figures S1 and S4 (Supporting Information) were performed on a Bruker Avance II 300 MHz spectrometer, equipped with a 5 mm QNP probe. The experiments shown in Figures 6 and 7 and in Figures S2 and S3 (Supporting Information) (^{1}H, DOSY and 2D NOESY) were performed on a Bruker Advance 400 spectrometer, operating at a frequency of 400.13 MHz and equipped with a 5 mm BBI probe with Z-gradient. The temperature was set to 298.15 K. All experiments were recorded using standard pulse sequences from the Bruker pulse library. DOSY spectra were recorded using Bruker's "ledbpgp2s" program by adjusting the parameters of diffusion delay (D) and gradient length (δ) for each sample. The gradient strength was varied from 2 to 95%. 2D NOESY spectra were recorded using Bruker's "noesyphpr" program, using mixing times of 500, 600, and 800 ms. For the spectra shown in Figures 5 and 8, 15 mg of dried sample A and 35.3 mg of dried sample B, were dissolved in 0.75 mL of deuterated chloroform. For Figure S1 (Supporting Information), 9.4 mg of dried sample C and 20.3 mg of dried sample D NCs were dissolved in 0.75 mL of deuterated chloroform. The total number of scans was 40. For the spectra shown in Figures 6 and 7 and in Figures S2 and S3 (Supporting Information), 17.6 mg of dried NCs dissolved in 0.75 mL of deuterated chloroform were used. The total number of scans was 16.

ICP analyses were carried out by digestion of 26 and 46 mg of NCs made of 0.1 and 0.2 mmol of Se at different stages of the reaction (1 and 2 min) in a mixture of hydrochloric and nitric acids. They were performed in a NexION 300 Mass Spectrometer with Inductively Coupled Plasma (ICP-MS), and the results are expressed in milligrams of element per milligrams of sample and summarized in Table S1 in the Supporting Information.

Elemental analysis of the supernatant upon SiO_2 coating (after sedimentation of the encapsulated NCs) was performed in a LECO CHNS-932 combusting 1 mg of the supernatant with two doses of oxygen (20 and 10 cm^3, respectively). The results can be found in Table S3 in the Supporting Information.

RESULTS AND DISCUSSION

Table 1 shows the details from the samples produced for this study: the initial ratio of the Cd and Se precursor's concentrations, the amount of DDT employed for the synthesis (see Experimental Section), the maximum wavelength of the PL peak, the PL QY, and the diameter of the NCs.

Table 1. Cd/Se Precursor Concentrations and Amount of DDT Employed in the Synthesis, Maximum Photoluminescence Emission Wavelength, Initial Quantum Yield, and Mean Diameter for Several Alloyed NCs

sample type	ratio Cd/Se	DDT (mmol)	PL (nm)	initial QY (%)	d (nm)
A	1:2	1	516	19.8 ± 0.2	7.5 ± 0.8
B	1:2	6	516	14.7 ± 0.1	7.5 ± 0.8
C	1:4	1	528	21.8 ± 0.1	5.2 ± 0.5
D	1:4	6	528	14.1 ± 0.1	5.2 ± 0.5

The two types of alloyed NCs (Cd/Se = 1:2 and Cd/Se = 1:4) have been produced under similar Cd and Zn but different Se precursor concentrations. Sample types A and B in Table 1 have been produced with half the Se concentration of types C and D. The amount of DDT has also been varied: 1 or 6 mmol for the two types of NCs.

As will be shown later, the variation in the Se concentration and DDT content leads to significant changes not only in the size and gradual composition of the NCs, but also in their reactivity against SiO_2 encapsulation.

Figure 1 shows the absorption and emission spectra of NCs type B and D, (1:2 and 1:4, respectively) along with TEM images. As can be observed, NCs produced under higher Se concentration, type C or D (Figure 1a,c) exhibit smaller sizes but, contrary to what is expected based on the quantum confinement effect, red-shifted optical response. Besides, NCs produced under lower Se precursor concentration, type A or B (Figure 1b,d) show larger sizes with shorter emission and band-edge wavelengths. Although the growth of smaller size NCs could be related to a higher amount of nuclei produced under Se excess conditions,[20] the shorter wavelength observed for larger NCs (types A and B) can be also explained by a mechanism, proposed by several authors, in which diffusion of elements from the outer shell (Zn) to the core takes place at the synthetic temperature (300 °C).[21,22] CdSe doping with Mn by thermodynamic controlled diffusion has also been previously studied.[23]

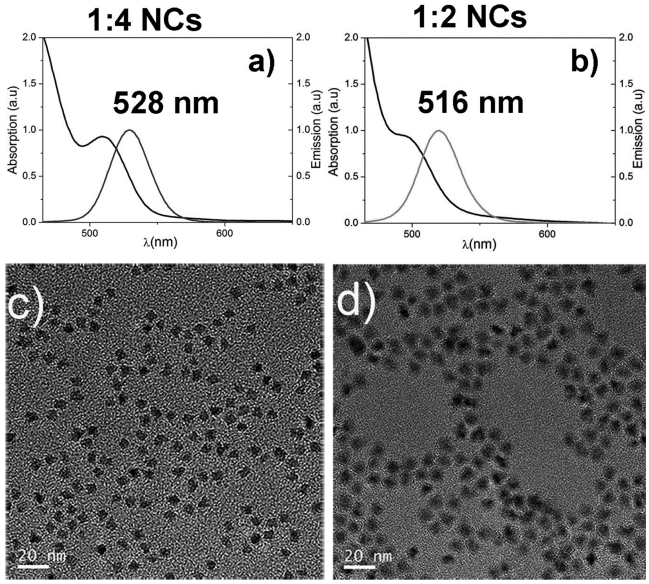

Figure 1. Absorption and emission spectra of (a) 1:4 type D and (b) 1:2 type B NCs. HRTEM images of (c) type D and (d) type B NCs.

Figure 2a shows the evolution of the PL peak of aliquots obtained at different times during the reaction at 300 °C, showing a clear blue-shift. In contrast, when the same reaction is performed at 260 °C the PL peak shifts in the opposite direction, as shown in Figure 2b. Thus, because diffusion is promoted at higher temperatures, the explanation to this blue-shift effect observed could be based on a feasible diffusion mechanism which will be the focus of future work. Nevertheless, for this study we have chosen samples produced exclusively at 300 °C due to their higher initial QY (≈ 20%) and produced after 2 min of reaction. As previously reported,[22] Zn migration also influences the particle shape, which can be explained by the fast interface alloying between CdSe and ZnS,

DOI: 10.1021/acsami.5b00820
ACS Appl. Mater. Interfaces 2015, 7, 6935−6945

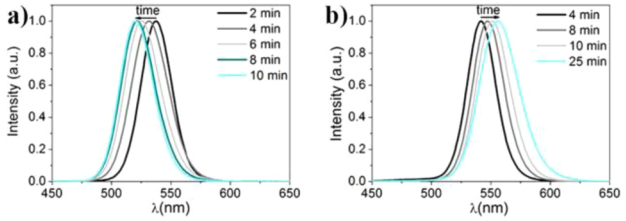

Figure 2. PL evolution of type D NCs synthesized at (a) 300 °C and (b) 260 °C, showing opposite trends. The blue-shift in graph a is related to the diffusion of Zn promoted at 300 °C, compared to the expected red-shift as the NCs grow observed at lower temperature (260 °C) in graph b.

corrupting the final structure. Evidence of this effect can be found in Figure 1 where a star-like or a degenerated tetrapod-structure rather than a spherical dot can be observed by TEM.

The remarkable differences in the optical properties of the two types of samples make further investigation of their surface chemistry essential. To investigate the gradual composition of the alloyed NCs, XPS measurements of the Cd 3d and Zn 3d core levels were performed using different photon energies, namely, 920 and 720 eV, which allows extraction of photoelectrons at different depths from the surface.[24−26] Table 2 gathers the XPS data recorded for the two types of

Table 2. Ratios Obtained from the Intensity of the XPS Peaks Taking into Account the Areas and the Integrating Times from the Surveys for Sample Types B and D

	1:2 type B	1:4 type D
Cd(920)/Cd(720)	2.8	
Zn(920)/Zn(720)	1.7	1.1

NCs. Because large (type A or B) and small (type C or D) NCs differ in the amount of DDT, just type B and D have been chosen as representatives samples for both sizes.

The values given correspond to the ratio between the areas of the different core levels. Because the ratio of the inelastic mean free paths for the Cd 3d core level measured at $h\nu$ = 920 eV and $h\nu$ = 720 eV is ∼1.35,[24] at 920 eV we extract information from deeper locations than at 720 eV. Although the difference is not very large, it is still significant because at 920 eV, Cd is detectable for both kinds of NCs, while at 720 eV, Cd is exclusively detectable for type B NCs. This indicates that NCs produced with higher Se concentration precursor (type D) are composed of a Cd rich core, while in type B NCs Cd is distributed in a more homogeneous way. Concerning the Zn distribution, the ratio between the inelastic mean free paths at 920 and 720 eV is somewhat smaller (i.e., ∼1.15), but the fact that the area ratio Zn(920)/Zn(720) is lower for type D samples points to a Zn rich surface compared to type B ones.

Thus, according to the TEM inspections and the XPS results, bigger NCs (type A and B) seem to be composed of a relatively homogeneous alloy, while in the smaller NCs (type C and D), which are also alloyed structures, a more defined core−shell structure can be identified, as sketched in Figure 3. This is relevant because the higher Cd content on the surface of type A/B samples (1:2 NCs) will promote better binding to the thiolated DDT ligand than the Zn sites.[17] ICP analysis of samples of both types of NCs can be found and discussed in the Supporting Information section (Table S1).

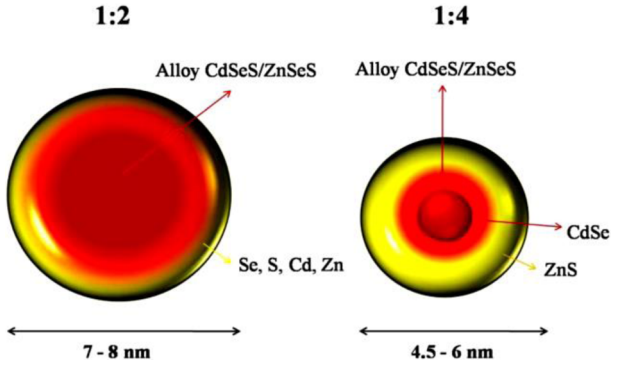

Figure 3. Sketches of the proposed structures for 1:2 (type A/B) and 1:4 NCs (type C/D).

SiO_2 Encapsulation of Alloyed NCs. The encapsulated NCs can be observed in the TEM images of Figure 4, where

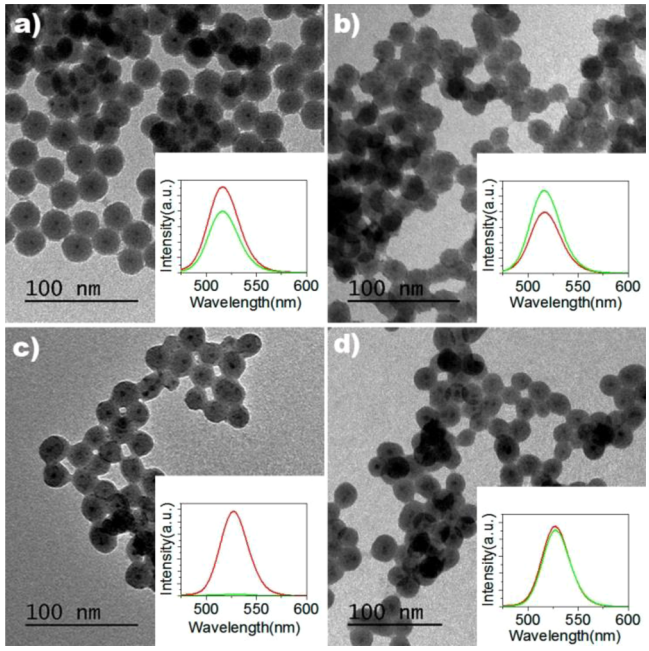

Figure 4. TEM images of SiO_2 encapsulated NCs for (a) sample A, (b) sample B, (c) sample C, and (d) sample D (see Table 1). (Insets) PL emission (red) before and (green) after being covered by SiO_2.

corresponding PL measurements are also included as insets. Table 3 shows information about the DDT content and the PL QY before and after SiO_2 encapsulation of representative samples of each type, A, B, C and D, along with a comment about the general luminescence behavior. (Statistics of

Table 3. QYs of 1:2 and 1:4 NCs with Different Amounts of DDT Added during Synthesis and Their QY before and after SiO_2 Coating

sample type	DDT (mmol)	QY before SiO_2	QY after SiO_2	PL behavior
A (1:2)	1	20	17	partial quenching
B (1:2)	6	15	16	preservation or increase of PL
C (1:4)	1	22	7	pronounced quenching
D (1:4)	6	15	15	preservation or slight increase of PL

DOI: 10.1021/acsami.5b00820
ACS Appl. Mater. Interfaces 2015, 7, 6935−6945

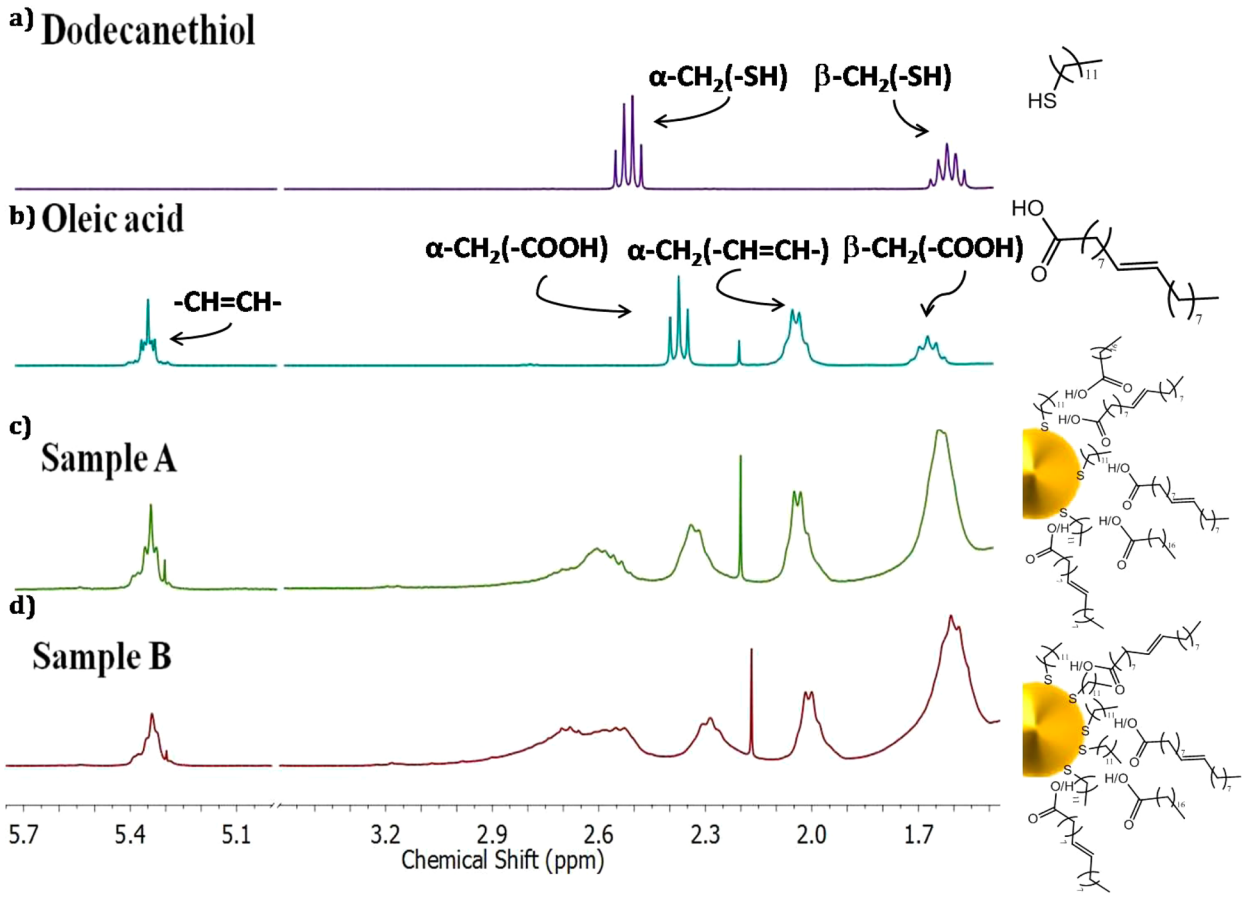

Figure 5. ^{1}H NMR spectra of (a) free DDT, (b) free OA, (c) 1:2 NCs treated with 1 mmol of DDT (sample A, Table 3) and (d) 6 mmol of DDT (sample B, Table 3) The sketches on the right depicts a ligand shell composed of tightly bounded DDT and weakly interpenetrated OA/SA molecules. (Singlets at around 2.15 ppm correspond to acetone).

additional 36 samples can be found in the Supporting Information, Table S2.) The luminescent properties were carefully measured in an integrating sphere (see Supporting Information for details). The results of Table 3 (and Table S2, Supporting Information) confirm that the SiO_2 coverage produces different results depending on the DDT amount added during the synthesis and on the initial precursor concentrations. In general, alloyed NCs treated with the highest amount of DDT exhibit lower initial PL QY (samples B-D vs A-C), in agreement with the Lewis base behavior of this ligand.[17] Upon SiO_2 coverage, type A samples produce partially quenched NCs.

Similar samples treated with higher DDT content (sample type B) exhibit in most cases lower initial QY, but upon coverage, the NCs are robust enough to prevent any drop in QY, and in many cases, slight enhancements are observed. Thus, it is clear that, although the DDT molecules have a well-known quenching effect on the initial PL properties of the alloyed NCs,[17] they seem to play an important role during the SiO_2 coverage process. This statement is further confirmed when analyzing the results obtained for the smaller NCs (samples type C and D). In this case, the treatment with a small amount of DDT generates samples with relatively high QY (up to 22%; sample type C). However, upon SiO_2 coverage, a pronounced quenching is systematically observed (Figure 4c and Table S2, Supporting Information). This strong effect is related to the higher relative surface area of smaller NCs, which requires higher DDT concentration to passivate the surface or that a higher amount of soft base DDT is required to effectively passivate the hard-acid Zn^{2+} shell. This result clearly explains the behavior of these NCs when treated with a higher amount of DDT (sample type D, Figure 4d). In this case, the initial QY remains constant or is increased upon SiO_2 coverage. Hence, it is clear that, although both types of NCs can be coated with SiO_2 without PL quenching, there is an optimum combination of ligands at their surface, depending on particle size and surface composition, that guarantees PL preservation.

To account for the mechanism underlying the SiO_2 coverage, we first analyzed the ligand sphere of the NCs by ^{1}H NMR (including DOSY and NOESY spectroscopy) and after each reactant addition during the reaction in microemulsion.

Figure 5 shows the ^{1}H NMR spectra of samples type A and B (treated with 1 and 6 mmol of DDT, respectively). For comparison, the spectra of free DDT and OA molecules in solution have also been included. Because OA and zinc stearate are used for the synthesis, it is possible that oleates, stearates, or their neutral forms, OA or SA, form part of the organic ligand shell. The DDT ^{1}H spectrum is characterized by two multiplets at 2.5 and 1.5 ppm corresponding to the protons of the methylene linked to sulfur in the α and β positions, respectively. The spectrum of free OA is composed of a multiplet corresponding to the olefinic protons of OA, centered at around 5.3 ppm, multiplets corresponding to the protons of the methylene groups linked to the acid group (around 2.3 ppm), to the unsaturation (around 2.0 ppm), and to the carboxylic acid in the α position at 1.6 ppm, apart from the

DOI: 10.1021/acsami.5b00820
ACS Appl. Mater. Interfaces 2015, 7, 6935−6945

signals related to the aliphatic chains that are not shown. The spectra of samples A and B show signals in several regions, namely, the range at 5.3 ppm, corresponding to the olefinic protons of OA, the region of the methylene group (α-CH_2) linked to sulfur around 2.6 ppm, the region around 2.0 ppm corresponding to α methylenes to the unsaturation, and the methylene groups in α and β positions to the carboxylic group of OA and/or SA ligands (around 2.3 and 1.6 ppm respectively). These spectra show that DDT, OA and/or SA are present on the NCs surface. In the case of OA, both position and width of the signals related to the unsaturation in free molecules and those interacting with the NCs surface are similar, suggesting a weak interaction of OA with the NCs surface.

Thus, OA may remain in the ligand sphere but, according to the relatively narrow and well-defined signal, not bounded to the NCs surface but probably interacting with the alkyl chains of the DDT molecules. The interdigitation of alkyl chains in the SiO_2 reaction has been previously reported.[3] The interaction between ligands is also suggested by the α-CH_2 group of OA/SA (range around 2.3), where there is a shielding (upfield signal) of those protons composing the ligand sphere of NCs with respect to the free OA. Rather than a bond to the surface, which would produce a downfield of the signal, the upfield is understood as a shielding effect produced by near DDT molecules that make the OA less sensitive to the magnetic field. Whether SA is also interpenetrated cannot be made out from these spectra. Its role in later SiO_2 coverage will be reported below. In contrast to the case of OA, the broad signals related to DDT (range around 2.6 ppm), compared to those observed for the free DDT molecules, suggest a strong interaction of DDT with the NCs surface. An increase in the intensity of the signal coming from the DDT bounded molecules when increasing concentration is clear when comparing samples treated with low and high DDT amounts (sample type A, Figure 5c, and type B, Figure 5d, respectively). Although this effect is more pronounced for the larger NCs, an increase in the intensity of the peaks related to anchored DDT molecules can also be observed for the smaller NCs, type C and D samples (Figure S1 in the Supporting Information).

To further elucidate the ligand shell composition, DOSY and NOESY spectra have been recorded.[27−32] The DOSY spectra of free OA, free SA, free DDT and NCs (sample B) can be seen in Figure 6. The signals of free DDT, OA and SA molecules correspond to diffusion coefficients of 1.1×10^{-9}, 8.1×10^{-10}, and 7.9×10^{-10} m^2/s, respectively.

These values are higher than the diffusion coefficient related to the NCs (3.4×10^{-10} m^2/s), indicating that all ligands diffuse together with the NCs. There are no signals showing diffusion coefficients similar to that of free OA. To clarify whether OA is actually anchored to the NCs surface or interacting with the ligand shell, extra amount of OA (10 μL) was added to the NCs dispersion.[27]

In this case, the ^1H signals related to OA protons increase their intensity, but not their width or chemical shifts (Figure S2 in the Supporting Information). The DOSY spectrum of this sample (sample B+OA in Figure 6) shows an intermediate diffusion coefficient between those of free ligands and NCs (4.5×10^{-10} m^2/s). This result suggests the incorporation of the extra OA in the NC ligand shell and rules out the presence of free OA in solution (at the amount employed).

The signals related to this sample containing extra OA diffuse faster than the NCs, which may point to an interaction between

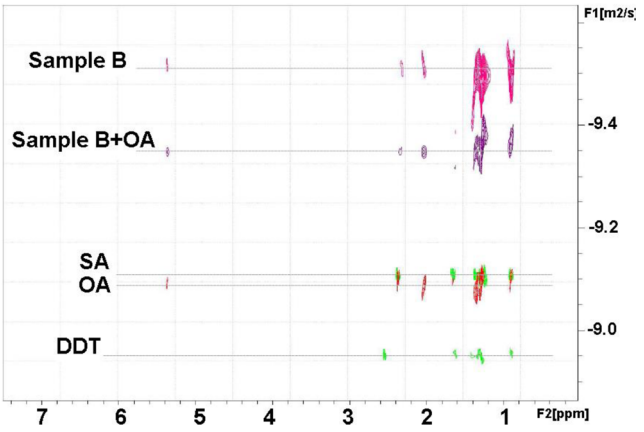

Figure 6. (Top to bottom) DOSY NMR spectra of sample B, sample B plus extra OA (B+OA), and free SA, OA, and DDT.

the alkyl chains of the molecules rather than a direct interaction with the NCs surface. To account for the intermolecular or intramolecular interactions between ligands, we performed NOESY experiments. Figure 7 shows the 2D NOESY spectra of the aliphatic regions of OA (panels a and c) and NCs sample B (panels b and d; the whole spectra can be found in the Supporting Information, Figure S3). The resonances related to methyl and methylenes show intense and positive NOEs, both for free OA and OA in the NC ligand sphere, discarding intermolecular interaction (compare panels a and b in Figure 7).

However, the α-and β-methylenes to the carboxylic group in the NCs spectra show a change in sign of cross peaks, compared with the free OA, and a weaker NOE effect (signals marked with the word "binding" in Figures 7b,d). This result clearly points to an intermolecular interaction where the carboxylic group of the intercalated OA must be close, but not directly anchored, to the NC surface, and the aliphatic part from the unsaturation (from C10) must be hanging from the outer part of the ligand shell. Thus, according to the NMR information, prior to encapsulation, the NCs are composed of tightly bounded DDT molecules and weakly bounded OA/SA, intercalated in the ligand shell, as schematically sketched on the right part in Figure 5.

To account for the mechanism underlying the SiO_2 coverage it is essential to understand the effect of both Igepal (as microemulsion surfactant) and TEOS additions. Figure 8b shows the ^1H NMR spectra of NCs (type B sample), and the spectra after Igepal (Figure 8c) and after TEOS addition (Figure 8d). For the sake of clarity, the OA spectrum is also shown (Figure 8a). As can be observed, the signal of OA in the sample is perturbed by the presence of Igepal, evidenced by an upfield of all signals (olefinic and α-methylene protons), indicating an interaction between the OA molecules and Igepal. Taking into account the chemical structure of both molecules, hydrogen bonds are feasible (see sketch on the right side of Figure 8). The addition of TEOS is identified by a further shift of all signals related to OA to lower frequencies. The move to shorter chemical shifts can be due to either the addition of an electropositive atom (Si from TEOS), or to a shielding effect provoked by the new molecule. Importantly, the signal related to the protons in the α-CH_2 of DDT remains in the same position after the addition of either Igepal or TEOS, indicating that the DDT molecules tightly bound to the NCs surface are not displaced from the surface and are not significantly affected

DOI: 10.1021/acsami.5b00820
ACS Appl. Mater. Interfaces 2015, 7, 6935−6945

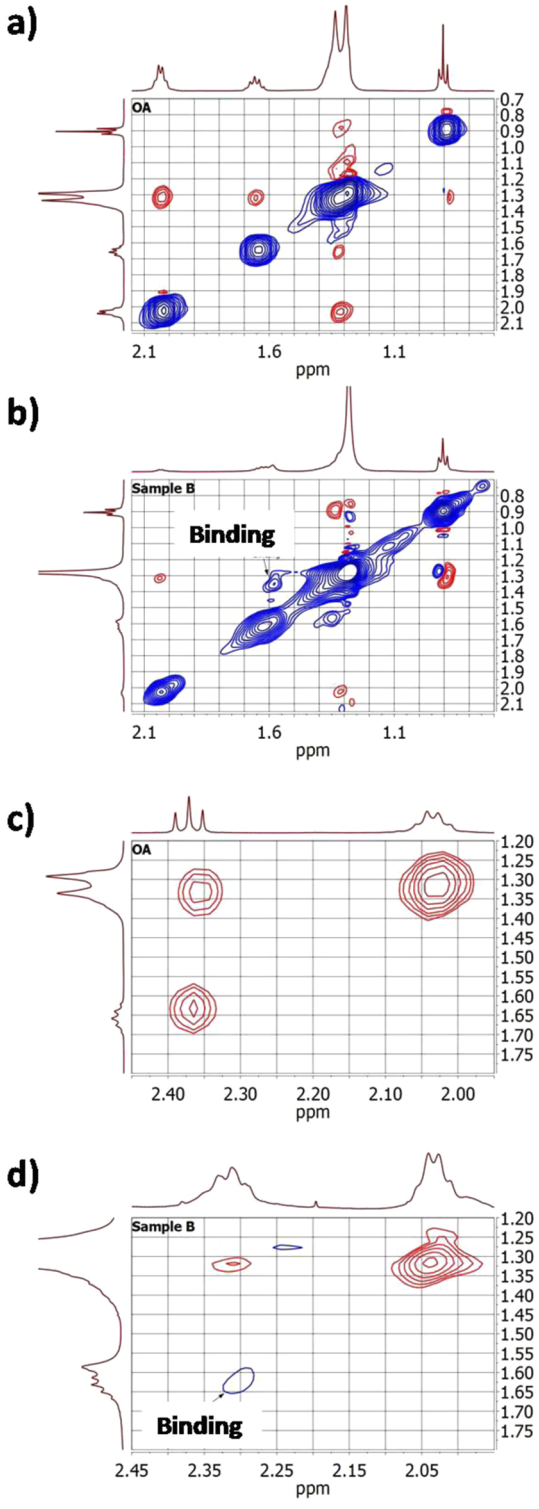

Figure 7. NOESY NMR spectra of (a and c) OA and (b and d) sample B showing the α-and β-methylenes to the carboxylic group in the NCs spectra show opposite sign compare to the free OA and weaker NOE effect. The change in sign of cross peaks indicates that OA interacts to NCs.

by them. This result shows that, for DDT capped NCs containing nonanchored OA, the silanization process may occur on the ligand shell, while the NCs surface remains protected from interacting with Igepal and TEOS. To account for any possible DDT or OA displacement after SiO_2 coating, the supernatant of the microemulsion was further analyzed. The spectrum shows main signals from Igepal and minor signals related to small amounts of OA (Figure S4 in the Supporting Information). Signals related to DDT molecules are not found, which confirms that these molecules are not displaced from the NCs surface upon SiO_2 coverage. Elemental analysis of the supernatant was also performed showing no sulfur content above the detection limit (Supporting Information Table S3).

In this way, a shell composed of tightly anchored DDT and a nonanchored or interdigitated OA/SA shell may prevent PL quenching, allowing for the SiO_2 reaction to take place in the ligand shell. Taking into account the above information, a mechanism as the one depicted in Chart 1 can be proposed.

As previously reported by Koole et al.,[10] thiol-capped NCs do not show any tendency to be covered by SiO_2 because the high affinity of thiolated molecules to the NCs surface prevents TEOS or Igepal ligand exchange, displacing the SiO_2 nucleation away from the NCs surface. On the contrary, Yang et al.[11] reported that water-soluble thioglycolic acid capped CdTe NCs can be encapsulated in microemulsion systems, which may indicate an active extra role of the carboxylic acid or differences between the slightly different hydrophilic character of the surfactants employed by those groups (5 versus 9.5 ethylene oxide units, respectively). In our case, the results show that no ligand exchange of DDT molecules takes place during the SiO_2 encapsulation process.

However, the results also indicate that, in the case reported here, these strongly bound ligands are necessary to maintain the initial optical properties, as they act as main anchoring points of OA/SA for the growing of the SiO_2 shell.

Apart from the lack of signals related to DDT in the ^1H NMR spectra of the microemulsion supernatant, further evidence pointing to a lack of DDT ligand exchange process with TEOS/Igepal can be deduced from PL decay measurements, where surface traps originated as a consequence of the ligand exchange are known to introduce nonradiative decay paths which alter the dynamics of the NCs emission. Figure 9 shows the decay curves and distribution of decay rates (Γ) for the different samples, along with details of the lifetime values (τ) before and after SiO_2 coating. The curves clearly show a multiexponential behavior pointing to a distribution of decay rates similar to recent observations on alloyed NCs.[33] Such distribution is due to fluctuating charge events at the single NC level and because we are simultaneously probing an ensemble of NCs with a distribution of morphologies. The best fit of the data, which yielded a quality of fit χ^2 close to 1, was obtained with a log-normal distribution of decay rates:[33]

$$I(t) = \int_0^\infty \rho(\Gamma)\, e^{-i\Gamma t} dt$$

where the decay distribution $\rho(\Gamma)$ is given by

$$\rho(\Gamma) = \frac{1}{\sigma\Gamma\sqrt{2\pi}}\, e^{-1/2\left(\frac{\ln\Gamma-\mu}{\sigma}\right)^2}$$

where Γ is the decay rate, and σ and μ the standard deviation and mean of its logarithm, respectively. (Additional optical details can be found in Table S4 in the Supporting Information) As can be seen in Figure 9a, type A samples show clearly different dynamics before and after coating, with an increased decay rate which is mainly related to nonradiative processes.

DOI: 10.1021/acsami.5b00820
ACS Appl. Mater. Interfaces 2015, 7, 6935−6945

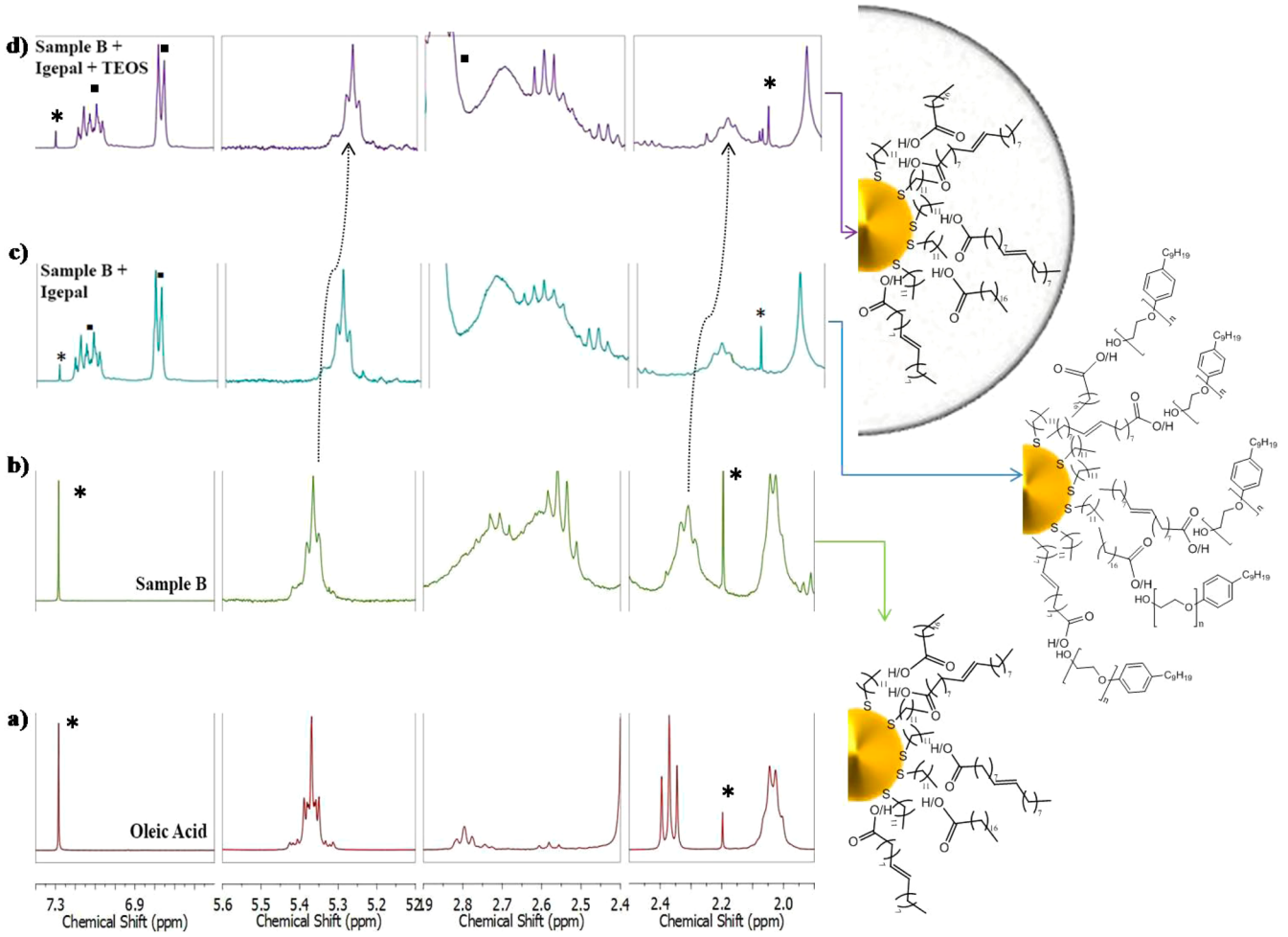

Figure 8. ^{1}H NMR spectra of (a) oleic acid (b) Sample B, (c) Sample B with Igepal CO-520, and (d) Sample B with Igepal CO-520 and TEOS; (*) solvents (chloroform and acetone), (■) Igepal CO-520.

Chart 1. Mechanism for SiO_2 Coating[A]

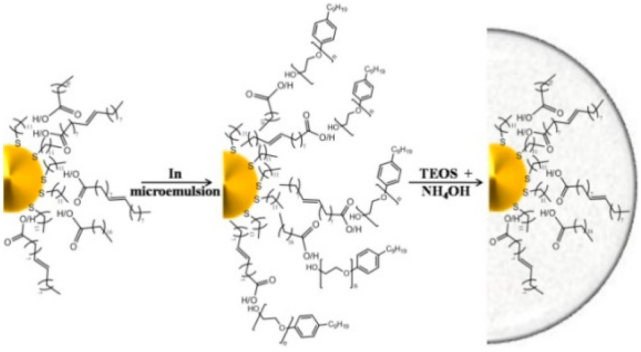

[A]In the first step, NCs with DDT ligands bound to the surface and interdigitated OA/SA ligands are introduced into the microemulsion system where they interact with Igepal molecules. In the second step the reaction of TEOS and NH_4OH takes place in the shell.

The concomitant decrease of PL (Figure 4a, inset) and lifetime values in these NCs points to a mechanism where all NCs are affected in a similar way by the coating process. (A decrease in the PL intensity maintaining the same exciton lifetime would be related to a process in which some NCs are quenched while others maintain the initial exciton lifetime values). From this information, it seems that type A samples are not well protected against the effects of SiO_2 coverage reaction. Type B samples, however, show rather identical dynamics and decay rates before and after coverage (Figure 9b). In this case, the DDT molecules form a protective ligand shell not affected by the SiO_2 growth that prevents ligand exchange on the surface. This result agrees with the PL emission peaks measured for type B samples where, as a general trend, the PL emission remains equal or increases upon SiO_2 coverage (Table 3 and Table S2, Supporting Information). In the case of type C samples, because their initial photoluminescent properties are severely affected after the treatment and the PL is quenched (Figure 4c, inset), dynamics and lifetime values are not included. In the case of type D samples (Figure 9c), although they have been produced under the same DDT concentration as type B samples, its smaller size (higher surface/volume ratio) and different surface chemistry (Zn rich) make the ligand shell not robust enough to maintain the initial photoluminescence properties, which can be seen in the reduced lifetimes of SiO_2 covered samples. Although the final QY of sample type D may be higher than B (due to a higher ligand density with respect to their size) the evolution of the decay dynamics with SiO_2 coverage show that type B samples exhibit the best protective ligand shells. This is related to two effects: (1) the smaller surface/volume ratio compared with C and D samples and (2) a better binding of DDT molecules to Cd surface sites, only

DOI: 10.1021/acsami.5b00820
ACS Appl. Mater. Interfaces 2015, 7, 6935−6945

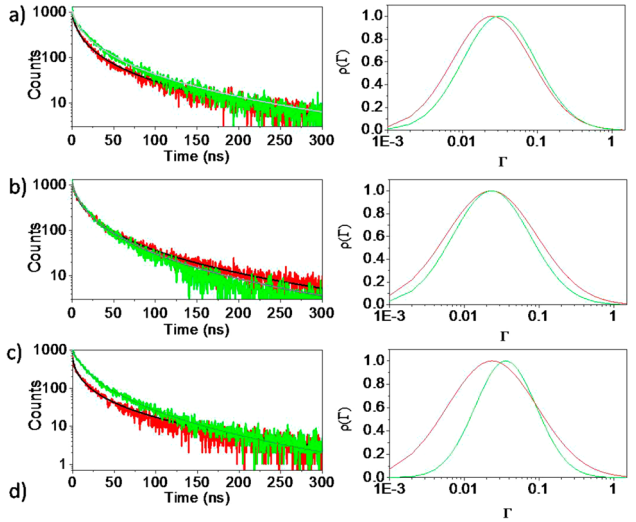

	τ (ns) Before SiO_2	τ (ns) After SiO_2
Sample type-A	40.1	32.1
Sample type-B	43.4	43.0
Sample type-D	42.1	27.8

Figure 9. Decay rates and log-normal distributions of NCs type (a) A, (b) B, and (c) D. Red (green) curves correspond to results before (after) SiO_2 coating. (d) Lifetime values of the NCs before and after coating.

present in A and B samples, according to the sketch proposed in Figure 3.

Thus, it is clear that, in order to prevent PL quenching, a ligand shell composed of anchored DDT ligands and intercalated OA/SA must be generated. This ligand shell will depend on the size and composition of the alloyed NCs. To provide further evidence of the proposed mechanism, we treated the samples described in Table 3 (types A, B, C and D) with extra amounts of OA/SA or DDT, depending on their size and ligand shell (Experimental Section). Because the ligand shell of types B and D samples is richer in DDT than types A and C, it is plausible to think that a simple post treatment with OA or SA before SiO_2 encapsulation will, at least, ensure the preservation of the initial PL QY. This was proven in a series of experiments where initial type B and D samples, with initial QYs between 13−22% and 14−24%, respectively, can reach QYs of 39% and 30% after SiO_2 coverage when incubated in OA (Table S5, Supporting Information). On the contrary, sample types A and C (poor DDT shell) do not show any improvement in QY after performing the same OA incubation procedure, pointing to a lack of DDT anchoring points. However, according to the proposed mechanism, the QY of these NCs should improve with previous incubation in DDT followed by OA or SA. The results of this experiment are illustrated in Figure 10. Figure 10a shows that poorly capped type C samples (whose PL was systematically quenched following the described SiO_2 coverage procedure) can maintain the initial PL properties (QY = 18%) if they are previously incubated first in DDT and later in OA. The QY of the final composite can even increase when the procedure includes SA, as shown in Figure 10b (QY = 28%). Special attention must be paid to the amount of DDT, since an excess of DDT provokes nucleation and growth of the beads out of NCs, according to the results reported by Koole et al.[10] (see Experimental Section for details). It is also worth noting that the size of the SiO_2 shell is smaller in the case of samples incubated in OA, according to

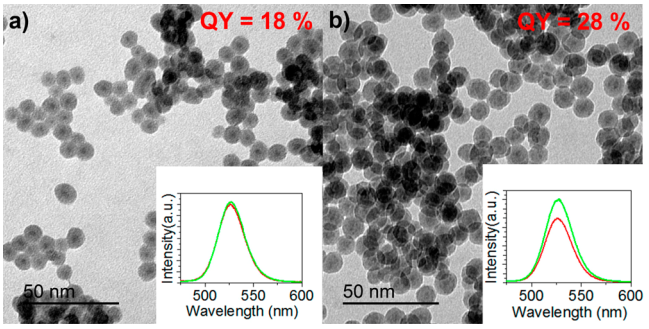

Figure 10. Type C NCs with initial QY of 18% incubated in DDT and further (a) OA or (b) SA prior to SiO_2 coverage. The insets show the PL peaks (red) before and (green) after SiO_2 growth. The QY is maintained in the first case and increases up to 28% in the second case.

a neutralizing effect of the acid in the ammonia catalyzed SiO_2 coverage reaction. Beads obtained under the same conditions are always smaller when using OA rather than SA, due to its higher acidity.

Considering the two main scenarios reported in the literature for the SiO_2 coverage reaction (either through ligand exchange on the NCs surface or through interactions of the microemulsion surfactant and the capping ligands of NCs) the results reported here indicate that a fine balance between surface chemistry and an adequate ligand shell may trigger the reaction through one or the other path. Our findings explicitly indicate that once the NCs surface is saturated with thiols, incubation with carboxylic acids will allow encapsulation in SiO_2, preserving or increasing the initial optical properties. The concentration of thiols depends on the size and, terminated atoms on the surface, as demonstrated with two different types of NCs. Because the carboxylic acid molecules get intercalated with the thiols (as stated by DOSY and NOESY spectroscopy), the amount of acid will also depend on the fraction of thiol ligands at the NCs surface.

CONCLUSIONS

In summary, in this work a study of the optical properties of alloyed CdSeZnS NCs upon SiO_2 coverage by microemulsion is reported. ^{1}H NMR including DOSY and NOESY spectroscopy has been used to elucidate the complex alloyed-NCs ligand shell composed of interpenetrated oleic/stearic acids in between tightly anchored dodecanethiol ligands, as well as the SiO_2 coverage mechanism. Because this shell prevents the PL quenching of the emitter, this information is very useful to understand variations in the PL QYs of different SiO_2 encapsulated NCs. The strongly bound dodecanethiol ligands are necessary to maintain the initial optical properties because they act as main anchoring points of oleic/stearic acids for the growing of the SiO_2 shell. This approach can be envisioned as a general method for the encapsulation of other types of NCs. The protective effect is related to nucleation and growth of the SiO_2 not on the NC surface but on the ligand shell. These results confirm that knowledge about the ligands and surface chemistry of the NCs is essential to explain and predict their further reactivity and optical properties, especially when alloyed structures are the target for encapsulation.

DOI: 10.1021/acsami.5b00820
ACS Appl. Mater. Interfaces 2015, 7, 6935−6945

■ ASSOCIATED CONTENT

Supporting Information

ICP-MS results; details on the measurements with an integration sphere and QYs of 1:2 and 1:4 NCs with the amount of DDT added during the synthesis and their QY before and after SiO_2 coating; ^1H NMR spectra of samples C and D and spectra of sample B and sample B with extra Oleic acid; NOESY spectra of sample B and OA; ^1H NMR spectrum of microemulsion supernatant; elemental analysis of microemulsion supernatant; details about the decay dynamics measurement and fittings; and information on quantum yields when NCs were previously incubated in oleic acid. This material is available free of charge via the Internet at http://pubs.acs.org.

■ AUTHOR INFORMATION

Corresponding Author

*E-mail: beatriz.hernandez@imdea.org, beatriz.hernandez@uam.es.

Present Address

[§]Instituto de Ciencia de Materiales de Sevilla, (ICMS), CSIC, Spain.

Notes

The authors declare no competing financial interest.

■ ACKNOWLEDGMENTS

The authors acknowledge the support from EU through NoE Nanophotonics4Energy grant 248855; the Spanish Ministry of Economy and Competitiveness through projects FIS2012-33011, MAT2012-31659, and MAT2013-47395-C4-3-R; and the Comunidad de Madrid through PHAMA_2.0. M.A. acknowledges IMDEA Nanoscience Foundation. D.G. acknowledges the Spanish Ministry of Economy and Competitiveness for RYC2012-09864.

■ REFERENCES

(1) Rogach, A. L. *Semiconductor Nanocrystal Quantum Dots. Synthesis, Assembly, Spectroscopy and Applications*. Springer−Wien: New York, 2008.

(2) Shao, L.; Gao, Y.; Yan, F. Semiconductor Quantum Dots for Biomedicial Applications. *Sensors.* **2011**, *11*, 11736−11751.

(3) Zhelev, Z.; Ohba, H.; Bakalova, R. Single Quantum Dot-Micelles Coated with Silica Shell as Potentially Non-Cytotoxic Fluorescent Cell Tracers. *J. Am. Chem. Soc.* **2006**, *128*, 6324−6325.

(4) Dubertret, B.; Skourides, P.; Norris, D. J.; Noireaux, V.; Brivanlou, A. H.; Libchaber, A. In Vivo Imaging of Quantum Dots Encapsulated in Phospholipid Micelles. *Science* **2002**, *298*, 1759−1762.

(5) Nann, T.; Mulvaney, P. Single Quantum Dots in Spherical Silica Particle. *Angew. Chem., Int. Ed.* **2004**, *43*, 5393−5396.

(6) Pietra, F.; van Dijk-Moes, R. J. A.; Ke, X.; Bals, S.; Van Tendeloo, G.; de Mello Donega, C.; Vanmaekelbergh, D. Synthesis of Highly Luminescent Silica-Coated CdSe/CdS Nanorods. *Chem. Mater.* **2013**, *25*, 3427−3434.

(7) Gerion, D.; Pinaud, F.; Williams, S. C.; Parak, W. J.; Zanchet, D.; Weiss, S.; Alivisatos, A. P. Synthesis and Properties of Biocompatible Water-Soluble Silica-Coated CdSe/ZnS Semiconductor Quantum Dots. *J. Phys. Chem. B* **2001**, *105* (37), 8861−8871.

(8) Li, C.; Murase, N. Formation Mechanism of Highly Luminescent Silica Capsules Incorporating Multiple Hydrophobic Quantum Dots with Various Emission Wavelengths. *J. Colloid Interface Sci.* **2013**, *411*, 82−91.

(9) Yang, P.; Murase, N.; Suzuki, M.; Hosokawa, C.; Kawasaki, K.; Katoz, T.; Taguchiz, T. Bright, Non-Blinking, and Less-Cytotoxic SiO_2 Beads with Multiple CdSe/ZnS Nanocrystals. *Chem. Commun.* **2010**, *46*, 4595−4597.

(10) Koole, R.; van Schooneveld, M. M.; Hilhorst, J.; de Mello Donegá, C.; Hart, D. C.; van Blaaderen, A.; Vanmaekelbergh, D.; Meijerink, A. On the Incorporation Mechanism of Hydrophobic Quantum Dots in Silica Spheres by a Reverse Microemulsion Method. *Chem. Mater.* **2008**, *20*, 2503−2512.

(11) Yang, Y. H.; Jing, L. H.; Yu, X. L.; Yan, D. D.; Gao, M. Y. Coating Aqueous Quantum Dots with Silica Via Reverse Microemulsion Method: Toward Size-Controllable and Robust Fluorescent Nanoparticles. *Chem. Mater.* **2007**, *19*, 4123−4128.

(12) Yang, Y.; Gao, M. Y. Preparation of Fluorescent SiO_2 Particles with Single CdTe Nanocrystal Cores by the Reverse Microemulsion Method. *Adv. Mater.* **2005**, *17*, 2354−2357.

(13) Hutter, E. M.; Pietra, F.; van Dijk, R. J. A.; Mitoraj, D.; Meldijk, J. D.; de Mello Donega, C.; Vanmaekelbergh, D. Method to Incorporate Anisotropic Semiconductor Nanocrystals of All Shapes in an Ultrathin and Uniform Silica Shell. *Chem. Mater.* **2014**, *26*, 1905−1911.

(14) Correa-Duarte, M. A.; Giersig, M.; Liz-Marzán, L. M. Stabilization of CdS Semiconductor Nanoparticles Against Photodegradation by a Silica Coating Procedure. *Chem. Phys. Lett.* **1998**, *286*, 497−501.

(15) Ma, X.; Tan, H.; Kipp, T.; Mews, A. Fluorescence Enhancement, Blinking Suppression, and Gray States of Individual Semiconductor Nanocrystals Close to Gold Nanoparticles. *Nano Lett.* **2010**, *10*, 4166−4174.

(16) Aubert, T.; Soenen, S.; Wassmuth, D.; Cirillo, M.; Deun, R.; Braeckmans, K.; Hens, Z. Bright and Stable CdSe/CdS@SiO_2 Nanoparticles Suitable for Long-Term Cell Labeling. *ACS Appl. Mater. Interfaces* **2014**, *6*, 11714−11723.

(17) De Mello Donega, C. Synthesis and Properties of Colloidal Heteronanocrystals. *Chem. Soc. Rev.* **2011**, *40*, 1512−1546.

(18) Sxorciapino, M. A.; Sanna, R.; Ardu, A.; Orru, F.; Casu, M.; Misuni, A.; Cannas, C. Core−Shell Nano-Architectures: The Incorporation Mechanism of Hydrophobic Nanoparticles into the Aqueous Core of a Microemulsion. *J. Colloid Interface Sci.* **2013**, *407*, 67−75.

(19) Bae, W. K.; Char, K.; Hur, H.; Lee, S. Highly Efficient Green-Light-Emitting Diodes Based on CdSe@ZnS Quantum Dots with a Chemical-Composition Gradient. *Adv. Mater.* **2009**, *21*, 1690−1694.

(20) Bae, W. K.; Char, K.; Hur, H.; Lee, S. Single-Step Synthesis of Quantum Dots with Chemical Composition Gradients. *Chem. Mater.* **2008**, *20*, 531−539.

(21) Panda, S. K.; Hickey, S. G.; Waurischa, C.; Eychmüller, A. Gradated Alloyed CdZnSe Nanocrystals with High Luminescence Quantum Yields and Stability for Optoelectronic and Biological Applications. *J. Mater. Chem.* **2011**, *21*, 11550−11555.

(22) Xia, X.; Liu, Z.; Du, G.; Li, Y.; Ma, M. Structural Evolution and Photoluminescence of Zinc-Blende CdSe-Based CdSe/ZnS Nanocrystals. *J. Phys. Chem. C* **2010**, *114*, 13414−13420.

(23) Vlaskin, V. A.; Barrows, C. J.; Erickson, C. S.; Gamelin, D. R. Nanocrystal Diffusion Doping. *J. Am. Chem. Soc.* **2013**, *135*, 14380−14389.

(24) Seah, M. P.; Dench, W. A. Quantitative Electron Spectroscopy of Surfaces: A Standard Data Base for Electron Inelastic Mean Free Paths in Solids. *Surf. Interface Anal.* **1979**, *1*, 2−11.

(25) Jablonsky, A.; Powell, C. J. The Electron Attenuation Length Revisited. *Surf. Sci. Rep.* **2002**, *47*, 33−91.

(26) Seah, M. P. Simple Universal Curve for the Energy Dependent Electron Attenuation Length for All Materials. *Surf. Interface Anal.* **2012**, *44*, 1353−1359.

(27) Fritzinger, B.; Capek, R. K.; Lambert, K.; Martins, J. C.; Hens, Z. Utilizing Self-Exchange to Address the Binding of Carboxylic Acid Ligands to CdSe Quantum Dots. *J. Am. Chem. Soc.* **2010**, *132*, 10195−10201.

(28) Gomes, R.; Hassinen, A.; Szczygiel, A.; Zhao, Q.; Vantomme, A.; Martins, J. C.; Hens, Z. Binding of Phosphonic Acids to CdSe

DOI: 10.1021/acsami.5b00820
ACS Appl. Mater. Interfaces 2015, 7, 6935−6945

Quantum Dots: A Solution NMR Study. *J. Phys. Chem. Lett.* **2011**, *2*, 145−152.
(29) Hens, Z.; Martins, J. C. A Solution NMR Toolbox for Characterizing the Surface Chemistry of Colloidal Nanocrystals. *Chem. Mater.* **2013**, *25*, 1211−1221.
(30) Hassinen, A.; Gomes, R.; De Nalf, K.; Zhao, Q.; Vantomme, A.; Martins, J. C.; Hens, Z. Surface Chemistry of CdTe Quantum Dots Synthesized in Mixtures of Phosphonic Acids and Amines: Formation of a Mixed Ligand Shell. *J. Phys. Chem. C* **2013**, *117*, 13936−13943.
(31) Malicki, M.; Knowles, K. E.; Weiss, E. A. Gating of Hole Transfer from Photoexcited PbS Quantum Dots to Aminoferrocene by the Ligand Shell of the Dots. *Chem. Commun.* **2013**, *49*, 4400−4402.
(32) Morris-Cohen, A. J.; Malicki, M.; Peterson, M. D.; Slavin, J. W.; Weiss, E. A. Chemical, Structural, and Quantitative Analysis of the Ligand Shells of Colloidal Quantum Dots. *Chem. Mater.* **2013**, *25*, 1155−1165.
(33) Ratchfor, D.; Dziatkowski, K.; Hartsfield, T.; Li, X.; Gao, Y.; Tang, Z. Photoluminescence Dynamics of Ensemble and Individual CdSe/ZnS Quantum Dots with an Alloyed Core/Shell Interface. *J. Appl. Phys.* **2011**, *109*, 103509.

DOI: 10.1021/acsami.5b00820
ACS Appl. Mater. Interfaces 2015, 7, 6935−6945